IEEE Access
Multidisciplinary ⋮ Rapid Review ⋮ Open Access Journal

Received January 9, 2022, accepted January 26, 2022, date of publication January 31, 2022, date of current version February 10, 2022.

Digital Object Identifier 10.1109/ACCESS.2022.3148325

Model Reference Adaptive Control of Cross-Coupling Hysteresis in Piezoceramics With Dynamic Loads

LUE ZHANG, ZIPENG ZHU, XIAOCHONG ZHOU, AND LINING SUN

Jiangsu Provincial Key Laboratory of Advanced Robotics, School of Mechanical and Electrical Engineering, Soochow University, Suzhou 215123, China

Corresponding author: Lue Zhang (zhanglve@suda.edu.cn)

This work was supported in part by the National Key Research and Development Program of China under Grant 2018YFB1304901, and in part by the National Natural Science Foundation of China under Grant 51505313.

ABSTRACT During the ultraprecise cutting of micro-structure surface with fast tool servo (FTS), the hysteresis of piezoelectric actuators (PEAs) are affected by dynamic voltage excitations and real-time cutting force, which declines the servo accuracy and cutting performance. In this paper, for a multi-input-single-output (MISO) cutting system, a cross-coupling rate-dependent Prandtl-Ishlinskii (CRPI) model is proposed and identified for the dynamic hysteresis of PEAs under dynamic voltage excitation and external loads. A model reference adaptive control method is then presented to eliminate the positioning nonlinearity of PEAs. The hysteresis modeling accuracy is discussed and the adaptive controller is validated through experiments.

INDEX TERMS Piezoelectric actuator, dynamic hysteresis model, cross-coupling, model reference adaptive control.

I. INTRODUCTION

In recent years, applications and demands of elements with functional and topologic micro-structure surface are increasing significantly. Fast tool servo (FTS) cutting is introduced to micro-structure surface ultraprecision manufacturing because of its fast frequency response and high machining accuracy. However, in FTS cutting process, the inherent hysteresis nonlinearity of piezoelectric actuator (PEA) and real-time cutting force from the workpiece, affect the tool servo performance of PEA, which declines the cutting surface quality. Moreover, due to the electro-mechanical coupling characteristics of piezoelectricity, hysteresis in FTS servo differs from those under static excitation and those without external loads. The changes of axial position, spindle speed and feed speed caused by the irregular surface morphology of the microstructure will affect the cutting efficiency [1], [2].

For the hysteretic characteristics of piezoceramics, various hysteresis models and control methods have been proposed [3]–[5]. To deal with the cross-coupling phenomenon in a hysteretic system, M. Rakotondrabe proposed a multi-variable model by introducing cross-coupling transfer operators into the classical Prandtl-Ishlinskii (PI) model [6]. Y. Dong *et al.* considered the influence of the external loads on the hysteresis and proposed a two-input Preisach model to estimate the cross-coupling hysteresis in PEAs under voltage excitation and external load in which, the distribution functions related to both voltage and load reflect the cross-coupled effect between the two inputs [7].

Furthermore, to describe the dynamic hysteresis under excitation with time-varying frequencies, rate-dependent PI model was proposed by employing dynamic weights or dynamic thresholds [8], [9], and its inverse compensation has shown satisfying accuracy for inputs at relatively lower frequencies [10].

Nevertheless, for higher exciting frequencies, the inverse operator might be invalid for severe nonlinearity, where the hysteretic curve slope is negative [6]. To enhance the application of rate-dependent PI model to inputs over a wider range of frequencies, hybrid control methods have been proposed. W. Li *et al.* proposed an online modeling method of rate-dependent hysteresis by introducing a nonlinear autoregressive moving average with exogenous inputs (NARMAX) model based on backpropagation (BP) neural network, an adaptive inverse controller was also developed with model inversion to suppress the hysteretic behavior of

The associate editor coordinating the review of this manuscript and approving it for publication was Yingxiang Liu.

This work is licensed under a Creative Commons Attribution-NonCommercial-NoDerivatives 4.0 License.
For more information, see https://creativecommons.org/licenses/by-nc-nd/4.0/

the actuator [11]. Y. Fan *et al.* purposed a radial basis function neural network (RBFNN) combined with rate-dependent PI model, and a disturbance observer was designed for wide-bandwidth tracking control of PEA system with input frequencies from 1 to 100 Hz [12].

Researches on hysteresis modeling and control have improved the driving accuracy of PEAs. Nevertheless, to control an FTS turning system, the electromechanical coupling characteristics of PEAs should be taken into consideration. In this paper, a cross-coupling rate-dependent Prandtl-Ishlinskii (CRPI) model is presented in Section II based on classical PI model, a model reference adaptive controller is proposed in Section III, experimental results and discussions for multi-hysteresis modeling and control are presents in Section IV.

II. CROSS-COUPLING RATE-DEPENDENT PRANDTL-ISHLINSKII MODEL

In this part, a cross-coupling rate-dependent Prandtl-Ishlinskii model is proposed to describe the hysteretic nonlinearities between the excited voltage, external load and the displacement of the PEA in a MISO system, and model parameters are identified subsequently.

A. DYNAMIC RATE-DEPENDENT PRANDLE–ISHLINSKII MODEL

In the FTS system, in order to offer the cutting tool a dynamic feeding rate for micro-structure surface machining, a voltage excitation with time-variant amplitude and frequency according to the designed tool path is necessary. In this case, to describe a precise relationship between dynamic voltage and output displacement of the PEAs, PI model is used. For the output of the classical PI model, hysteresis nonlinearity is approached by summation of a series of weighted backlash operators with different thresholds. The backlash operator is shown as followed

$$\begin{aligned} y(t) &= F_r[u, y_0](t) \\ &= \max\{u(t) - r, \min[u(t) + r, y(t - T)]\} \\ y(0) &= \max\{u(t) - r, \min[u(t) + r, y_0]\} \end{aligned} \tag{1}$$

where u is the operator input, F_r is the operator function, T is the sampling period, $y(t)$ is the operator output, $y(t-T)$ is the operator output of previous time, r is the threshold value.

Then the hysteretic nonlinearity can be expressed as:

$$z(t) = H_r[u](t) = \sum_{i=0}^{n} w_i F_r[u, y_0](t) = \boldsymbol{w}^T \boldsymbol{F}_r[u, y_0](t) \tag{2}$$

where $\boldsymbol{w}^T = [w_0 \cdots w_n]$ is the transposition vector matrix of weight; $\boldsymbol{r} = [r_0 \cdots r_n]^T$ is the vector matrix of threshold; $\boldsymbol{F}_r[u, y_0](t) = [F_{r0}[u, y_0](t) \cdots F_{rn}[u, y_0](t)]$ is the vector matrix of operator.

The displacement hysteretic loop of the PEA increases with the frequency of the excitation signal [13], [14]. To model the dynamic hysteresis of PEA, the static weights of classical PI model are extended by introducing the change rate of excitations. The dynamic weight is denoted as

$$\boldsymbol{w} = \boldsymbol{k} \cdot \dot{u}(t) + \boldsymbol{b} \tag{3}$$

where $\boldsymbol{k} = [k_1, k_2, \cdots k_n]^T$ is the slope matrix of dynamic input, $\boldsymbol{b} = [b_1, b_2, \cdots b_n]^T$ is the offset coefficient matrix of dynamic input, $\dot{u}(t)$ is the rate of change of input signal. Then the rate-dependent PI model for dynamic hysteresis can be described as

$$z(t) = H_r[u](t) = \sum_{i=0}^{n} [k_i \cdot \dot{u}(t) + b_i] \cdot F_r[u, y_0](t) \tag{4}$$

B. CROSS-COUPLING DYNAMIC PRANDLE–ISHLINSKII MODEL

During micro-structure surface cutting process, the dynamic feeding rate of FTS system causes changes not only in cutting depth but also in corresponding cutting force, which introduces modeling error to hysteretic characteristics of (4) and affects the positioning accuracy of PEAs due to piezoelectricity effect.

For a PEA system with exciting voltage $u(t)$ and external load $F(t)$, the arithmetic unit $\boldsymbol{H}[\cdot]$ is introduced to relate $u(t)$ and $F(t)$ to the output displacement $z(t)$ of the PEA and the structure can be shown in Fig. 1:

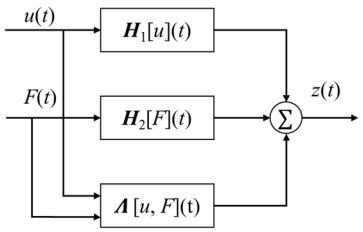

FIGURE 1. The structure of the cross-coupling dynamic PI model.

When the load is zero, the arithmetic unit can be equivalent to the dynamic hysteresis characteristic $H_1[u](t)$ of the PEA with voltage excitation:

$$z_u(t) = H_1[u](t) \quad for\ F(t) = 0 \tag{5}$$

When the voltage is zero, the arithmetic unit can be equivalent to the dynamic hysteretic characteristic $H_2[F](t)$ of the PEA with load excitation:

$$z_F(t) = H_2[F](t) \quad for\ u(t) = 0 \tag{6}$$

Hysteretic characteristic of the PEA displacement under load excitation is also rate dependent, so the dynamic rate-dependent PI model established in the previous section can be used to represent $H_1[u](t)$ and $H_2[F](t)$:

$$H_1[u](t) = \sum_{i=0}^{n} w_1^i \cdot y(u, t) = \sum_{i=0}^{n} [k_i \cdot \dot{u}(t) + b_i] \cdot y(u, t) \tag{7}$$

$$H_2[F](t) = \sum_{i=0}^{n} w_2^i \cdot y(F, t) = \sum_{i=0}^{n} [m_i \cdot \dot{F}(t) + c_i] \cdot y(F, t) \tag{8}$$

where $y(u,t)$ and $y(F,t)$ can be obtained according to (1); m is the slope of H_2 to be identified; c is the migration coefficient of dynamic threshold to be identified.

The cross-coupling effect between relations of voltage-displacement and load-displacement is denoted by $\mathbf{\Lambda}[u, F](t)$, which can be approximated by a Back-Propagation (BP) neural network with the structure indicated in Fig.2.

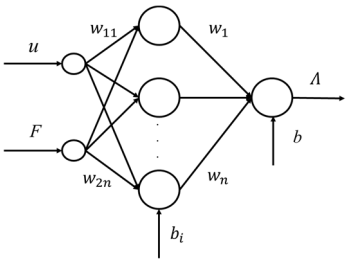

FIGURE 2. Neural network structure of cross-coupling hysteresis.

Define transfer function of the neural network as a sigmoid function, the coupled displacement can be expressed as

$$\mathbf{\Lambda}[u, F](t) = f[\sum_{i=1}^{n} w_i f(w_{1i}u + w_{2i}F + b_i) + b] \quad (9)$$

where w_{1i} $(i = 1, 2 \ldots n)$ is the weight and b_j is the threshold from the input layer to the hidden layer, w_i is the weight and b is the threshold from the hidden layer to the second layer, $f(x)$ is the transfer function, n is the number of hidden layer nodes.

Therefore, the cross-coupling dynamic PI model can be expressed as

$$z(t) = H[u, F](t) = H_1[u](t) + H_2[F](t) + \mathbf{\Lambda}[u, F](t) \quad (10)$$

C. PARAMETER IDENTIFICATION

Since the cross-coupling dynamic PI model consists of three parts: $H_1[u](t)$, $H_2[F](t)$ and $\Lambda[u, F](t)$, the parameter identification requires both weight value solving process in the dynamic PI model and the neural network training process. The parameters to be identified include the slope and offset coefficient in the dynamic weight of (7) and (8), the weight value w_i and threshold value b_i in each layer of the network.

With least squares method (LSM), the parameter identifications for $H_1[u](t)$ and $H_2[F](t)$ are similar. Therefore, only the process of parameter identification for $H_1[u](t)$ is presented in detail as follows:

1) Experimental data acquisition: for $j = 1, 2, \ldots, m$, where m is the number of measured data, apply a voltage excitation $u(t_j)$ to PEA, and take the measured displacement as $z_a(t_j)$;
2) Threshold determination: the threshold value r in the backlash operator is given by

$$r_i = \frac{i}{n} |u_{\max} - u_{\min}|, \quad i = 0, 1 \cdots n-1 \quad (11)$$

where n is the number of thresholds, $u_{\max}$ and $u_{\min}$ are the maximum and minimum input voltage.

3) Modeling displacement prediction: according to (7) and (11), the predicted nonlinear displacement output of the model is given by $z(t)$;
4) Objective function determination: by comparing modeling output $z(t)$ to experimental displacement $z_a(t)$, the objective function J is given by

$$J = \frac{1}{m}\sum_{j=1}^{m}[z(t_i) - z_a(t_j)]^2 = \frac{1}{m}\sum_{j=1}^{m}\{\boldsymbol{w}^T \boldsymbol{F}_r[u, y_0](t_j) - z_a(t_j)\}^2 \quad (12)$$

5) Parameter identification with the objective function minimization.

With parameters of $H_1[u](t)$ and $H_2[F](t)$ verified, the cross-coupling parameters w_{1i}, w_{2i}, b_i, w_i, and b are determined by neural network learning and modifications. The steepest descent backpropagation (SDBP) algorithm is used and the specific process can be referred to [15].

III. MODEL REFERENCE ADAPTIVE CONTROL

To control the above hysteretic performance of PEA, a model reference adaptive controller is proposed. For a system with output displacement x, reference model output x_{m} and tracking error e_{m}, the schematic diagram is shown in Fig. 3.

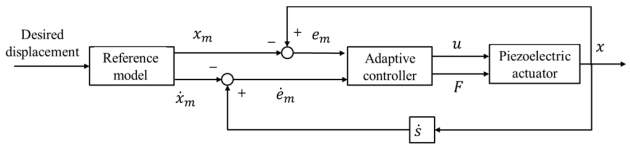

FIGURE 3. Block diagram of a model reference adaptive control system.

Based on the tracking error e_{m} between reference model and the actual output, the controller is schemed by adaptive law designing and parameter tuning with system robustness balanced.

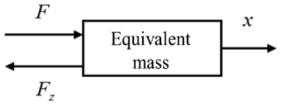

FIGURE 4. Dynamic model of a PEA.

The adaptive control law is designed according to the dynamic model of piezoelectric actuator under voltage and load shown in Fig. 4. The dynamic equation of a PEA can be established as

$$m\ddot{x} = F - F_z \quad (13)$$

where m is the equivalent mass of PEA; F_z denotes the equivalent force of the voltage.

When a PEA is excited by voltage, the force produced by its displacement $z(t)$ can be expressed as

$$F_z(t) = k_s z(t) = k_s H[u, F](t) \quad (14)$$

where k_s is the stiffness coefficient.

Therefore, (13) can be rewritten as

$$m\ddot{x} = F - F_u = F - k_s H[u, F](t) \tag{15}$$

And $\ddot{x}$ is

$$\ddot{x} = \frac{F}{m} - \frac{k_s}{m} H[u, F](t) \tag{16}$$

Defining $K_E = k_s/m$, $\ddot{x}$ can be rewritten as

$$\ddot{x} = \frac{F}{m} - K_E H[u, F](t) \tag{17}$$

Assuming the reference output together with its 1st- and 2nd-order derivatives are all bounded, to design an adaptive control system with an output approaching x_m gradually, the following steps are taken with regard to [16].

Because the controller is designed according to the error and its derivative between the reference model output and the actual output of PEA, error function needs to be obtained firstly; then a Lyapunov function is constructed and the control law is analyzed and deduced; consequently, effectiveness of the controller is proved by Barbarat theorem. The design process of controller is presented in the following part.

Firstly, the error function e is defined by

$$e = x - x_m, \quad \dot{e} = \dot{x} - \dot{x}_m \tag{18}$$

To introduce a function determined by e and $\dot{e}$, Lyapunov function $V_1 = \frac{1}{2}e^2$ is defined, and its derivative can be expressed as

$$\dot{V}_1 = e\dot{e} = e(\dot{x} - \dot{x}_m) \tag{19}$$

By defining $e_1 = \dot{x} - \alpha$ with $\alpha = -ke + \dot{x}_m$, and k is a positive constant, e_1 is introduced to associate e, $\dot{x}$ and $\dot{x}_m$. (19) can be rewritten as

$$\dot{V}_1 = e(\dot{x} - \dot{x}_m) = e(e_1 + \alpha - \alpha - ke) = ee_1 - ke^2 \tag{20}$$

Combined with the dynamic model, the derivative of e_1 is

$$\dot{e}_1 = \ddot{x} - \dot{\alpha} = \frac{1}{m}F - K_E H[u, F](t) + ke_1 - k^2 e - \ddot{x}_m \tag{21}$$

Subsequently, a Lyapunov candidate function is given by

$$V_2[e(t), e_1(t)] = V_1 + \frac{1}{2}e_1^2 \tag{22}$$

The derivative of V_2 is

$$\dot{V}_2[e(t), e_1(t)] = \dot{V}_1 + e_1\dot{e}_1 = ee_1 - ke^2 + e_1\dot{e}_1 \tag{23}$$

According to (21), the adaptive control law is designed as follows

$$K_E H[u, F](t) = e - k^2 e + ke_1 + se_1 - \ddot{x}_m + \frac{F}{m} \tag{24}$$

where s is a positive constant. The control voltage and control load can be expressed as follows:

$$u = H_u^{-1}\left[\frac{e - k^2 e + ke_1 + se_1 - \ddot{x}_m + \frac{F}{m}}{K_E}\right](t) \tag{25}$$

$$F = H_F^{-1}\left[\frac{e - k^2 e + ke_1 + se_1 - \ddot{x}_m + \frac{F}{m}}{K_E}\right](t) \tag{26}$$

where H_u^{-1} is the voltage inversion of H, H_F^{-1} is the load inversion of H. They can be described by rate-dependent PI operators as

$$H_u^{-1}[z](t) = \sum_{i=0}^{n-1} w_i'[\dot{u}(t)] \cdot F_{r'}[z](t) \tag{27}$$

where the expression of $F_{r'}$ is the same as F_r. The weights w' and the thresholds r' in H_u^{-1} can be obtained by the following equations:

$$r_i' = \sum_{j=0}^{i} w_j[\dot{u}(t)](r_i - r_j) \tag{28}$$

$$\begin{cases} w_0'[\dot{u}(t)] = \dfrac{1}{w_0[\dot{u}(t)]} \\ w_i'[\dot{u}(t)] = \dfrac{-w_i[\dot{u}(t)]}{\sum_{j=0}^{i} w_j[\dot{u}(t)] \sum_{j=0}^{i-1} w_j[\dot{u}(t)]} \end{cases} \tag{29}$$

Substituting (25) and (26) into (21), the following equation can be obtained:

$$\begin{aligned} \dot{e}_1 &= \frac{F}{m} - (e - k^2 e + ke_1 + se_1 - \ddot{x}_m \\ &\quad + \frac{F}{m}) + ke_1 - k^2 e - \ddot{x}_m \\ &= -e - se_1 \end{aligned} \tag{30}$$

Then,

$$\dot{V}_2 = -ke^2 - se_1^2 \leq 0 \tag{31}$$

Therefore $V_2[e(t), e_1(t)] \leq V_2[e(0), e_1(0)]$, which implies $e(t)$ and $e_1(t)$ are bounded.

Define $W(t) = ke^2 + se_1^2$, then

$$\int_0^t W(\tau)d\tau \leq V_2[e(0), e_1(0)] - V_2[e(t), e_1(t)] \tag{32}$$

Since $V_2[e(0), e_1(0)]$ is bounded while $V_2[e(t), e_1(t)]$ is nonincreasing and bounded, we can obtain:

$$\lim_{t\to\infty} \int_0^t W(\tau)d\tau < \infty \tag{33}$$

According to Barbalat lemma [17], for $t \to \infty$, e and e_1 converge to zero, therefore the stability of the model reference adaptive control system can be guaranteed.

IV. EXPERIMENT RESULTS

In this part, to verify the CRPI model and control method proposed in previous section, experimental platform is setup for the hysteretic characteristic testing, and simulation control platform is established based on MATLAB/Simulink. For a PEA under voltage and load excitations with fixed or time-varying frequencies, experiments are carried out for both the rate-dependent hysteresis modeling and the model reference adaptive control performance, related results are presented and discussed respectively.

A. VERIFICATION AND ANALYSIS OF HYSTERESIS MODEL

The experimental platform is shown in Fig 5, in which two piezoelectric actuators: one serves as the servo PEA to be controlled for dynamic hysteresis, and other one is used for the purpose of dynamic load supplying.

A voltage excitation generated by signal generator (Trueform 33500B) and amplified by the modular piezoelectric controller (Core Tomorrow, E00. A4), is applied to the tested PEA (Physik Instrumente, P-841.6). With integrated strain sensor, actuator displacement is obtained from controller module (Physik Instrumente, E-518), then data acquisition and processing of external load are carried out (Physik Instrumente, PI MikroMove).

Another piezoelectric actuator (Core Tomorrow, Pst150/7/20 VS12) indicated in Fig. 5 provides the tested PEA with dynamic force, which is determined by

$$F_{PZT} = (x_l - x_a)k_s \tag{34}$$

where x_l and x_a are theoretical and measured actuator displacement respectively.

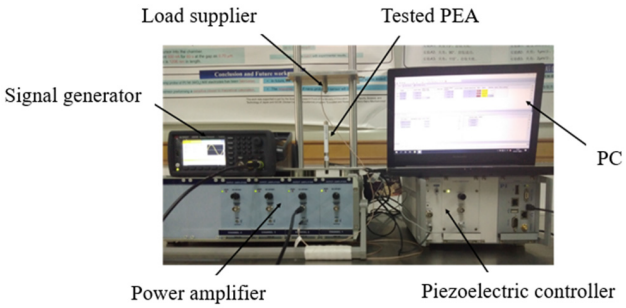

FIGURE 5. Experimental platform.

In microstructure surface cutting process, reaction of the dynamic cutting force on the tool is normally regarded as a disturbance to system feeding, as presented in our previous work, for the same voltage excitation, a deflection can be observed between the output hysteresis loops of a PEA with and without external load [15].

It should also be noted that, for FTS ultraprecise turning, both the tool feeding and dynamic cutting force are smaller than traditional cutting. In this work, to verify the modeling and control accuracy experimentally, a sinusoidal voltage signal $u(t) = 50\sin 2\pi ft$ ($f = 5$Hz, 20Hz, 50Hz and 100Hz) and a sinusoidal load with the same amplitude and frequency are applied to the piezoelectric actuator. The experimental data and the modeling output at different frequencies are shown in Fig. 6. It can be observed that modeling outputs fit the experimental curve well for lower frequencies, while modeling error increases for higher input frequencies such as 100Hz.

Table 1 shows the average errors and corresponding root mean square errors (RMSE) between the cross-coupling rate-dependent model and the measured curve in Fig. 6. With the presented modeling errors, performance of above CRPI model can be validated for the rate-dependent hysteresis of a piezoelectric actuator in a MISO system with fixed input frequency.

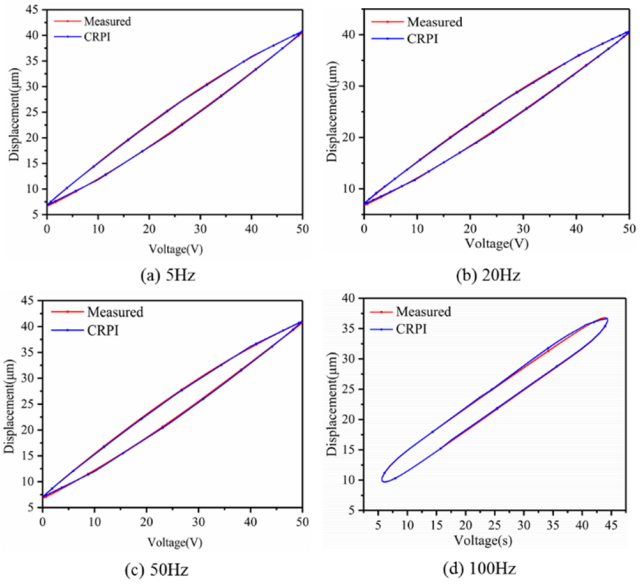

FIGURE 6. The measured and modeled hysteresis curves with different exciting frequencies.

TABLE 1. The output errors of CRPI model at different frequencies.

Frequency (Hz)	Average error (μm)	RMSE (μm)
5	0.1175	0.0931
20	0.1727	0.1672
50	0.3402	0.2514
100	0.5013	0.3618

For further verification of CRPI modeling accuracy, a dynamic excitation signal, as indicated in Fig. 7(a), is generated and applied to the piezoelectric actuator. The hysteresis curves of modeling and measured displacements are shown in Fig. 7 (b). With an average modeling error of 0.5854μm and RMSE of 0.6207μm, the CRPI model performs sufficient modeling accuracy under both static and dynamic excitations.

B. VERIFICATION AND ANALYSIS OF MODEL REFERENCE ADAPTIVE CONTROLLER

For a model reference adaptive controller, the controller parameters are iterated by the constant comparison between the measured and expected actuator displacements. In this part, the controller is determined and verified with experimental platform shown in Fig. 5.

The control system is built in MATLAB/Simulink according to the adaptive control law (25) and (26) proposed in the previous section. With an expected displacement, PEA output and its error are calculated to obtain a control signal, which is a digital signal that should be converted by D/A module

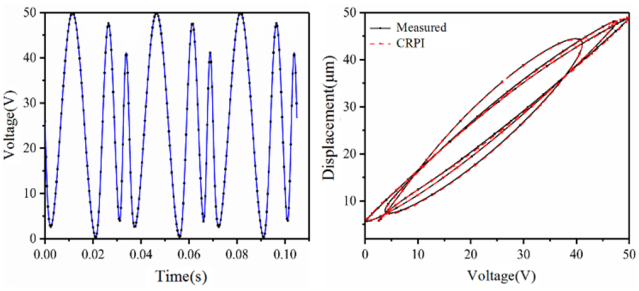

(a)A generated dynamic voltage signal (b) Measured and modeled hysteresis

FIGURE 7. Modeled and measured hysteresis curves under a dynamic excitation.

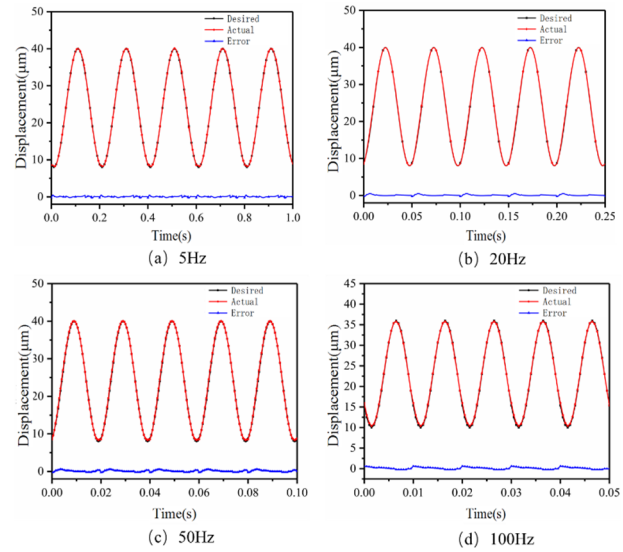

FIGURE 8. The expected and controlled displacements with different exciting frequencies.

of data acquisition card (PCI-1716). Subsequently, amplified by piezoelectric controller, the control signal is applied to PEA, while PEA output is measured by an integrated strain sensor and acquired by sensor module of piezoelectric controller. After A/D conversion, the converted digital displacement signal is transmitted to the Desktop Real-Time module of Simulink, and then continuously processed in control module.

The controller parameters are determined in the following part. A general second-order model is selected as the reference model indicated in Fig. 3. With the System Identification Toolbox of MATLAB, a general transfer function is identified according to the expected input and output data imported. The estimated transfer model is given by

$$G(s) = \frac{3040}{s^2 + 28s + 3040} \tag{35}$$

In experiments, the stiffness coefficient of piezoelectric actuator is $k_s = 60\text{N}/\mu\text{m}$. Therefore, parameters of the model reference adaptive controller to be identified are k and s. A step input signal is used for parameter tuning. Initially, a step size of 5 is taken for $5 < k < 50$ and a step size of 0.1 is taken

TABLE 2. Control errors for excitations at different frequencies.

Frequency (Hz)	Average error (μm)	RMSE (μm)
5	0.0674	0.1048
20	0.1775	0.1835
50	0.1982	0.3594
100	0.3017	0.3819

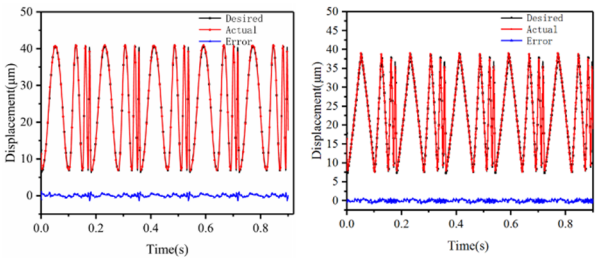

(a) Dynamic sinusoidal signal (b) Dynamic triangle signal

FIGURE 9. Expected displacements and the controlled displacements under dynamic excitations.

for $0.1 < s < 10$, to seek for minimum stability time and overshoot. By adjusting step sizes, an optimized controller is obtained with a stability time of 0.02s and overshoot about 0.8%, when $k = 21$, $s = 2.8$.

When the desired displacement signals are sinusoidal signals with 5Hz, 20Hz, 50Hz and 100Hz respectively, the controller parameters are $k = 21$, $s = 2.8$, $k_s = 60\text{N}/\mu\text{m}$. The controlled displacement and controlling errors are illustrated in Fig. 8 and Table 2 respectively, which show the hysteretic nonlinearity of piezoelectric actuator can be well restrained by the proposed model reference adaptive controller.

For expected displacements under dynamic excitations, experimental results of the controlled outputs and corresponding errors are shown in Fig. 9. For a dynamic sinusoidal signal with time-vary frequency, the average output error of is $0.2163\mu\text{m}$, the RMSE is $0.3085\mu\text{m}$; for a dynamic triangle signal, the average error and RMSE is $0.1548\mu\text{m}$ and $0.3167\mu\text{m}$ respectively. Therefore, the validity of the proposed model reference adaptive controller can be verified.

V. CONCLUSION

In this paper, to eliminate the hysteretic nonlinearity of PEA under dynamic excitations in applications such as FTS microstructure surface cutting, a rate-dependent PI model is improved by employing dynamic weights for multi-hystereses, and a cross-coupling rate-dependent PI hysteresis model is proposed for the coupled mechanical and electrical characteristics of piezoelectric material. Meanwhile, to makeup the decline of CRPI compensation accuracy for higher exciting frequencies, a model reference adaptive controller is developed where a general second-order system is taken as reference model. The design of corresponding adaptive control law is presented, and its stability and convergence

are proved by Lyapunov function. The proposed model and controller are both verified by experiments. In future, offline parameter identification of the cross-coupling dynamic PI model will be further optimized to improve modeling and control accuracy.

REFERENCES

[1] A. B. Taylor, P. Michaux, A. S. M. Mohsin, and J. W. M. Chon, "Electron-beam lithography of plasmonic nanorod arrays for multilayered optical storage," *Opt. Exp.*, vol. 22, no. 11, pp. 13234–13243, Jun. 2014.

[2] R. Huang, X. Zhang, M. Rahman, A. S. Kumar, and K. Liu, "Ultra-precision machining of radial Fresnel lens on roller moulds," *CIRP Ann.*, vol. 64, no. 1, pp. 121–124, 2015.

[3] Y. Chen, Q. Huang, H. Wang, and J. Qiu, "Hysteresis modeling and tracking control for piezoelectric stack actuators using neural-preisach model," *Int. J. Appl. Electromagn. Mech.*, vol. 61, no. 3, pp. 445–459, Nov. 2019.

[4] F. Ikhouane, "A survey of the hysteretic Duhem model," *Arch. Comput. Methods Eng.*, vol. 25, no. 4, pp. 965–1002, Nov. 2018.

[5] M. Al Janaideh, M. Rakotondrabe, and O. Aljanaideh, "Further results on hysteresis compensation of smart micropositioning systems with the inverse Prandtl–Ishlinskii compensator," *IEEE Trans. Control Syst. Technol.*, vol. 24, no. 2, pp. 428–439, Mar. 2016.

[6] M. Rakotondrabe, "Multivariable classical Prandtl–Ishlinskii hysteresis modeling and compensation and sensorless control of a nonlinear 2-dof piezoactuator," *Nonlinear Dyn.*, vol. 89, no. 1, pp. 481–499, Jul. 2017.

[7] Y. Dong, H. Hu, and H. Wang, "Identification and experimental assessment of two-input Preisach model for coupling hysteresis in piezoelectric stack actuators," *Sens. Actuators A, Phys.*, vol. 220, pp. 92–100, Dec. 2014.

[8] W. T. Ang, P. K. Khosla, and C. N. Riviere, "Feedforward controller with inverse rate-dependent model for piezoelectric actuators in trajectory-tracking applications," *IEEE/ASME Trans. Mechatronics*, vol. 12, no. 2, pp. 134–142, Apr. 2007.

[9] M. Al Janaideh and P. Krejci, "Inverse rate-dependent Prandtl–Ishlinskii model for feedforward compensation of hysteresis in a piezomicropositioning actuator," *IEEE/ASME Trans. Mechatronics*, vol. 18, no. 5, pp. 1498–1507, Oct. 2013.

[10] Y. Qin, X. Zhao, and L. Zhou, "Modeling and identification of the rate-dependent hysteresis of piezoelectric actuator using a modified Prandtl–Ishlinskii model," *Micromachines*, vol. 8, no. 4, p. 114, Apr. 2017.

[11] W. Li and X. Chen, "Compensation of hysteresis in piezoelectric actuators without dynamics modeling," *Sens. Actuators A, Phys.*, vol. 199, pp. 89–97, Sep. 2013.

[12] Y. Fan and U.-X. Tan, "Design of a feedforward-feedback controller for a piezoelectric-driven mechanism to achieve high-frequency nonperiodic motion tracking," *IEEE/ASME Trans. Mechatronics*, vol. 24, no. 2, pp. 853–862, Apr. 2019.

[13] J. Chen, G. Peng, H. Hu, and J. Ning, "Dynamic hysteresis model and control methodology for force output using piezoelectric actuator driving," *IEEE Access*, vol. 8, pp. 205136–205147, 2020.

[14] G.-Y. Gu, L.-M. Zhu, and C.-Y. Su, "Modeling and compensation of asymmetric hysteresis nonlinearity for piezoceramic actuators with a modified Prandtl–Ishlinskii model," *IEEE Trans. Ind. Electron.*, vol. 61, no. 3, pp. 1583–1595, Mar. 2014.

[15] X. Zhou, L. Zhang, Z. Yang, and L. Sun, "Modeling and inverse compensation of cross-coupling hysteresis in piezoceramics under multi-input," *Micromachines*, vol. 12, no. 1, p. 86, Jan. 2021.

[16] J. Ling, Z. Feng, M. Ming, and X. Xiao, "Model reference adaptive damping control for a nanopositioning stage with load uncertainties," *Rev. Sci. Instrum.*, vol. 90, no. 4, Apr. 2019, Art. no. 045101.

[17] H. Jahanshahi, A. Yousefpour, J. M. Munoz-Pacheco, S. Kacar, V.-T. Pham, and F. E. Alsaadi, "A new fractional-order hyperchaotic memristor oscillator: Dynamic analysis, robust adaptive synchronization, and its application to voice encryption," *Appl. Math. Comput.*, vol. 383, Oct. 2020, Art. no. 125310.

LUE ZHANG received the Ph.D. degree in mechatronics engineering from the Harbin Institute of Technology, China, in 2012.

She is currently an Associate Professor with the Mechanical and Electrical Engineering School, Soochow University. Her current research interests include micro/nano positioning, nonlinear control, and acoustics manipulation.

ZIPENG ZHU received the bachelor's degree from Nanjing Forestry University, Nanjing, China, in 2021. He is currently pursuing the master's degree with the Mechanical and Engineering School, Soochow University.

His research interests include nonlinear control of piezoceramic and trajectory control.

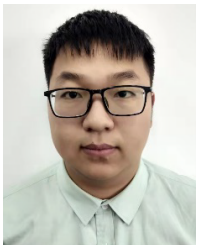

XIAOCHONG ZHOU received the bachelor's degree from Soochow University, Suzhou, China, in 2018, where he is currently pursuing the master's degree with the Mechanical and Electrical Engineering School.

He is working on nonlinear control of piezoceramic in micro/nano scale.

LINING SUN received the Ph.D. degree in mechatronics engineering from the Harbin Institute of Technology, China, in 1993.

He is currently a Professor with the Mechanical and Electrical Engineering School, Soochow University. His research interests include robotic control, micro and nanorobotics, micromanipulation, nanopositioning actuators, and design and control of high-speed nanopositioning systems.